Supplementary document for

Fracture toughness of fly ash-based geopolymer gels: Evaluations using nanoindentation experiment and molecular dynamics simulation

Gideon A. Lyngdoh[1], Sumeru Nayak[1], N.M. Anoop Krishnan[2,3,*], and Sumanta Das[1,*]

[1]Department of Civil and Environmental Engineering, University of Rhode Island, Kingston, RI, USA

[2]Department of Civil Engineering, Indian Institute of Technology Delhi, Hauz Khas, New Delhi, 110016, India

[3]Department of Materials Science and Engineering, Indian Institute of Technology Delhi, Hauz Khas, New Delhi, 110016, India

[*]Corresponding authors: N. M. A. Krishnan (krishnan@iitd.ac.in), S. Das (sumanta_das@uri.edu)

A. Evaluation of radial cracks during indentation using extended finite element method

The fracture toughness evaluated from indentation experiment heavily relies on the choice of the indenter geometry and the crack morphologies such as median crack, radial crack, half-penny crack, or lateral cracks [1,2]. Visualization of cracks via x-ray tomography (XRT) or SEM for highly heterogeneous materials is challenging and cracks often close after withdrawal of indenter. To ensure if radial cracks (beyond contact area) are actually formed, a method as explained in [3] is adopted where the onset and the propagation of radial crack is tracked by detecting the discontinuities in the P-C_c plot. Here P is the indentation load and C_c is defined as: $C_c = \frac{dP}{d(h^2)}$; where h is the indentation depth. Figure 1(a) shows a representative load-penetration depth plot for N-A-S-H and Figure 1(b) plots the P-C_c relationship, obtained from load-penetration depth plot. The first peak in Fig. 1(b) (vertical line (i)) indicates the onset of crack and further increase in load causes the crack to propagate, indicated by the undulations obtained beyond a penetration depth of 400 nm. Hence, this analysis ensures the formation and propagation of radial crack during indentation.

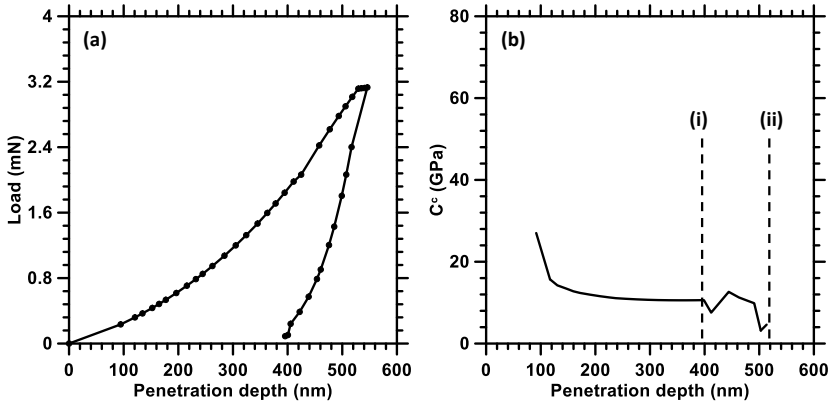

Figure 1: (a) Representative P (load) vs h (penetration depth) relationship for N-A-S-H obtained from nanoindentation experiment, (b) C_c vs h relationship: The vertical line-(i) indicates onset of crack and line-(ii) signifies the maximum penetration depth

To evaluate the influence of the length of radial cracks on the obtained fracture toughness of N-A-S-H, a numerical simulation using extended finite element method are carried out. In this analysis, a sufficiently large (as compared to the size of the nanoindenter) cylindrical sample of diameter $10\ \mu m$ and thickness $5\ \mu m$ is modelled for nanoindentation simulation. The material model for N-A-S-H phase is adopted as elastic-plastic model. For simplicity, a perfect elastic-plastic material behavior is assumed i.e., the strain hardening exponent is equal to zero, the stress will not increase once the yielding occurs at the yield stress. For boundary condition, a base of the substrate is restrained from vertical and horizontal directions and C3D8 element type is implemented in this simulation. The contact between the substrate and the

indenter is assumed to be frictionless. To obtain the response from the simulation, a displacement control and a loading-unloading protocol is applied to the indenter with the maximum applied displacement equal to 0.5 µm. For indenter, a rigid Berkovich pyramidal indenter (centerline-to-face angle of 65.3°) contacting the surface is adopted. The crack propagation is modelled using extended finite element model (XFEM) where a maximum principal stress criterion is used for crack-initiation and fracture energy was used for crack propagation. The details of XFEM method can be found in [4–6].

While the fracture energy of N-A-S-H can be adopted as the one obtained from MD simulations and the Young's modulus obtained from nanoindentation can be directly used for N-A-S-H, the intrinsic strength of N-A-S-H is not readily available in the literature. Hence, we adopted an inverse analysis approach to determine the strength of N-A-S-H from the strength of the geopolymer paste, obtained from split tensile strength experiments on the same material using the same synthesis and curing conditions explained in the paper. From the split tensile strength experiments, we obtained a value of 1.85 ± 0.052 MPa (σ_{max}). The inverse analysis approach is shown in Figure 2.

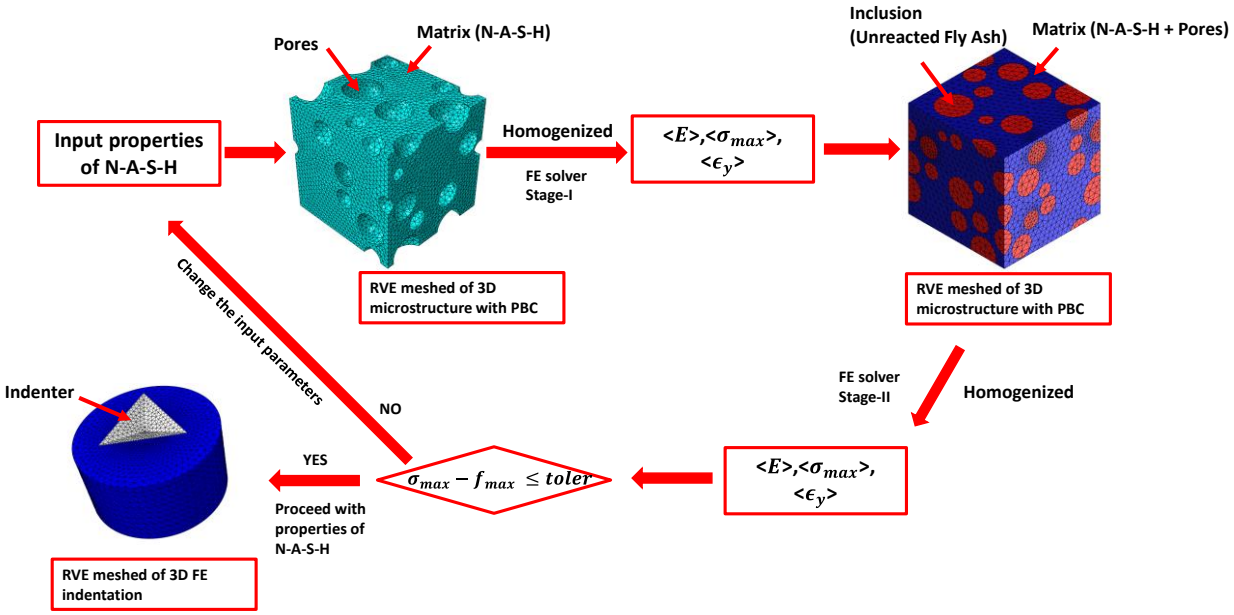

Figure 2. A workflow used to obtain the tensile strength of N-A-S-H from known tensile strength of geopolymer paste.

The inverse analysis starts with an assumption of tensile strength of N-A-S-H. In the first step, pores are homogenized with N-A-S-H to obtain homogenized properties which serve as matrix properties in the next scale where the remaining fly ash particles are homogenized in the matrix to obtain the geopolymer paste strength from FEA (f_{max}). The analysis is performed using Abaqus software package [7] and MATLAB [8]. The error between σ_{max} and f_{max} is minimized using an iterative process as shown in Figure 2 to finally

obtain the tensile strength of N-A-S-H which serve as input for nanoindentation simulation, explained hereafter. In the multiscale simulation process, the sizes of unit cells (shown in Figure 3) are chosen carefully after an RVE-size sensitivity study. Also, an optimal mesh was incorporated after a detailed mesh convergence study.

The relative volume fractions of constituent phases are directly adopted from our previous studies [9,10] where the volume fractions were determined using synchrotron x-ray tomography and scanning electron microscopy (SEM). The intrinsic Young's modulus of N-A-S-H and remaining fly ash are obtained from nanoindentation experiments as shown in this paper. Here, unreacted fly ash, partially activated fly ash and fly ash with cavities are first analytically homogenized using Mori-Tanaka method [11] to obtain the homogenized Young's modulus of fly ash for simplicity. Similar approach was also adopted in our previous work [9]. Using the above-mentioned inverse analysis approach, a tensile strength of 3.03 MPa was obtained for N-A-S-H which serves as input for XFEM simulation.

For indentation simulation, the parameters used for XFEM simulation are provided in table 1.

Table1: Input parameters for XFEM simulation

E (GPa)	ν	Max. Principal stress (MPa)	Fracture energy (N/mm)
18	0.25	3.03	0.01

Here an optimal mesh with number of 200077 elements (C3D8 elements in ABAQUS™) is chosen after detailed mesh-convergence study which is shown in Figure 3.

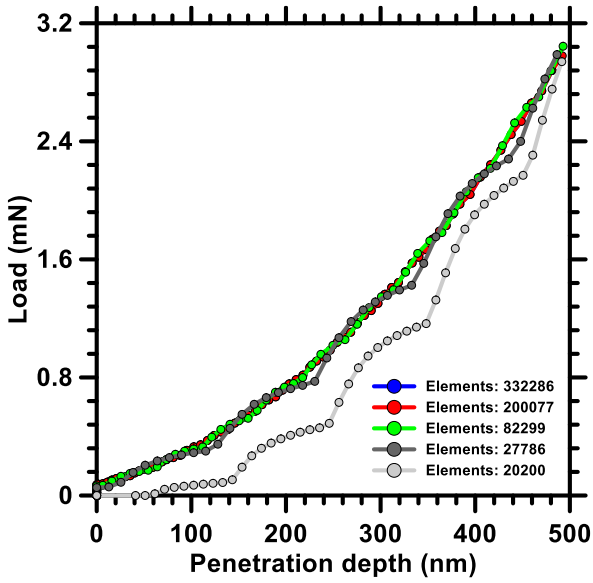

Figure 3: Mesh convergence results during loading in load-penetration depth

Figure 4(a) shows the simulated and the experimental load-penetration depth relationship where the simulated response shows excellent match with the experimental data, thus validating the XFEM analysis. Figure 4(b) shows the maximum principal stress for the maximum penetration depth. Subset of the figure shows a zoomed location of a small radial crack. Thus, this analysis proves our hypothesis on the smaller size of radial crack. Figure 4(c) shows the displacement contours during indentation. After obtaining the radial crack length profiles with increasing penetration depth from the XFEM simulation, the fracture area can now be obtained as: $A_{fr} = 6at + \Sigma dl_i dt_i + \Sigma dl_j dt_j + \Sigma dl_k dt_k$. Here the indices i, j and k correspond to the three radial cracks extended from three sharp corners of the Berkovich indenter. The calculated A_{fr} from XFEM simulation, which includes the influence of radial cracks (7.56 μm^2), is slightly higher as compared to the adopted A_{fr}in this paper, as expected due to the contribution of the radial cracks.

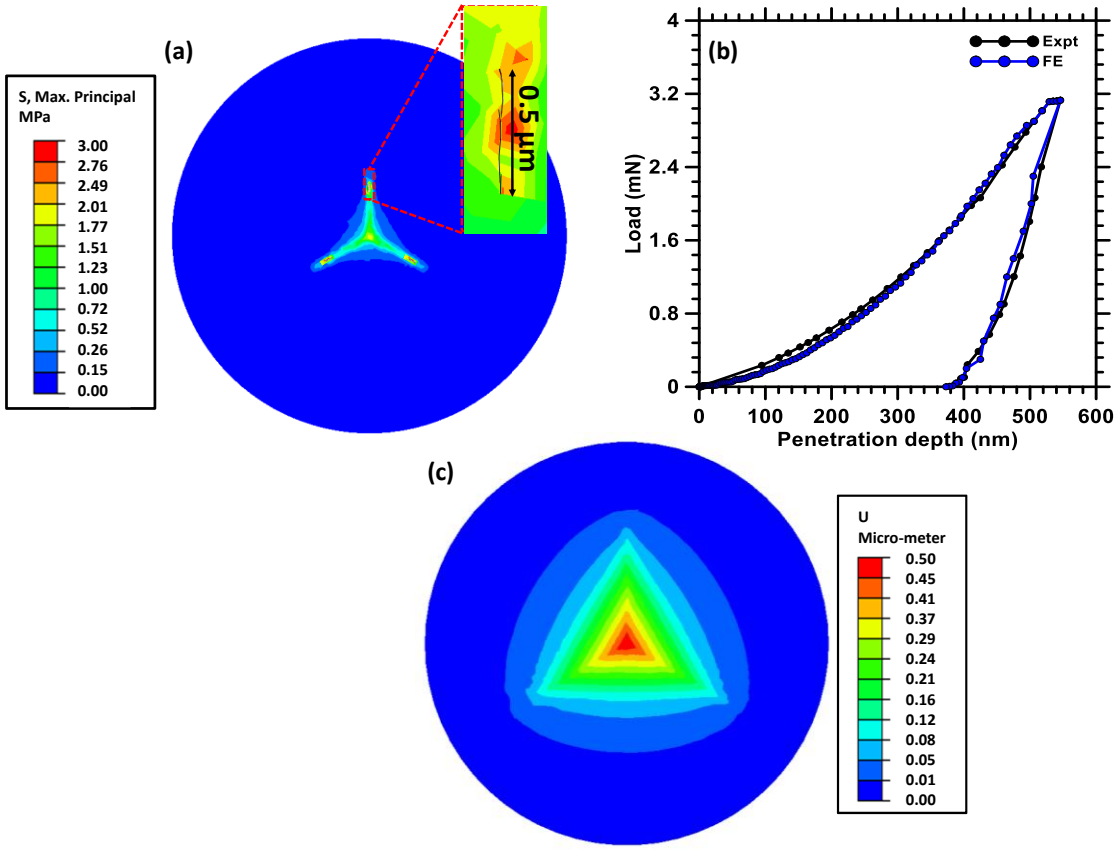

Figure 4 (a) Maximum principal stress distribution obtained from FE analysis, (b) comparison of the P vs H curve between simulated data and experimental data, (d) displacement plot from simulated nanoindentation analysis.

Overall, the calculated fracture toughness (including the radial cracks) is 0.46 MPa-m$^{0.5}$ which is not significantly different as compared to the obtained fracture toughness of 0.485 MPa-m$^{0.5}$ from

nanoindentation which doesn't consider the influence of the radial cracks due to the challenges explained earlier. Thus, the XFEM simulation results prove that in case of nanoindentation experiments on quasi-brittle materials using Berkovich indenter, the influence of radial crack extensions beyond the contact area on the fracture toughness computation is not very significant and as such, the small radial crack extensions in quasi-brittle materials do not affect the total fracture area significantly during indentation.

B. Reactive Forcefield for N-A-S-H

Reactive MD-force field: c/h/o/water/Al/Si/Fe (Pitman et al., JACS 2012)

```
 39      ! Number of general parameters
 50.0000 !Overcoordination parameter
  9.5469 !Overcoordination parameter
  1.6725 !Valency angle conjugation parameter
  1.7224 !Triple bond stabilisation parameter
  6.8702 !Triple bond stabilisation parameter
 60.4850 !C2-correction
  1.0588 !Undercoordination parameter
  4.6000 !Triple bond stabilisation parameter
 12.1176 !Undercoordination parameter
 13.3056 !Undercoordination parameter
-55.1978 !Triple bond stabilization energy
  0.0000 !Lower Taper-radius
 10.0000 !Upper Taper-radius
  2.8793 !Not used
 33.8667 !Valency undercoordination
  6.0891 !Valency angle/lone pair parameter
  1.0563 !Valency angle
  2.0384 !Valency angle parameter
  6.1431 !Not used
  6.9290 !Double bond/angle parameter
```

```
  0.3989 !Double bond/angle parameter: overcoord
  3.9954 !Double bond/angle parameter: overcoord
 -2.4837 !Not used
  5.7796 !Torsion/BO parameter
 10.0000 !Torsion overcoordination
  1.9487 !Torsion overcoordination
 -1.2327 !Conjugation 0 (not used)
  2.1645 !Conjugation
  1.5591 !vdWaals shielding
  0.1000 !Cutoff for bond order (*100)
  1.7602 !Valency angle conjugation parameter
  0.6991 !Overcoordination parameter
 50.0000 !Overcoordination parameter
  1.8512 !Valency/lone pair parameter
  0.5000 !Not used
 20.0000 !Not used
  5.0000 !Molecular energy (not used)
  0.0000 !Molecular energy (not used)
  0.7903 !Valency angle conjugation parameter
  9    ! Nr of atoms; cov.r; valency;a.m;Rvdw;Evdw;gammaEEM;cov.r2;#
         alfa;gammavdW;valency;Eunder;Eover;chiEEM;etaEEM;n.u.
         cov r3;Elp;Heat inc.;n.u.;n.u.;n.u.;n.u.
         ov/un;val1;n.u.;val3,vval4
C    1.3817   4.0000  12.0000   1.8903   0.1838   0.9000   1.1341   4.0000
     9.7559   2.1346   4.0000  34.9350  79.5548   5.9666   7.0000   0.0000
     1.2114   0.0000 202.6057   8.9539  34.9289  13.5366   0.8563   0.0000
    -2.8983   2.5000   1.0564   4.0000   2.9663   1.2000   0.2000  13.0000
H    0.8930   1.0000   1.0080   1.3550   0.0930   0.8203  -0.1000   1.0000
     8.2230  33.2894   1.0000   0.0000 121.1250   3.7248   9.6093   1.0000
```

-0.1000 0.0000 61.6606 3.0408 2.4197 0.0003 1.0698 0.0000

-19.4571 4.2733 1.0338 1.0000 2.8793 1.0000 0.2000 12.0000

O 1.2450 2.0000 15.9990 2.3890 0.1000 1.0898 1.0548 6.0000

9.7300 13.8449 4.0000 37.5000 116.0768 8.5000 8.3122 2.0000

0.9049 0.4056 59.0626 3.5027 0.7640 0.0021 0.9745 0.0000

-3.5500 2.9000 1.0493 4.0000 2.9225 1.3000 0.2000 13.0000

Fe 1.9506 3.0000 55.8450 2.0308 0.1274 0.7264 -1.0000 3.0000

11.0534 2.2637 3.0000 0.0000 18.3725 1.2457 7.3021 0.0000

-1.2000 0.0000 66.4838 30.0000 1.0000 0.0000 0.8563 0.0000

-16.2040 2.7917 1.0338 6.0000 2.5791 1.3000 0.2000 13.0000

Cl 1.7140 1.0000 35.4500 1.9139 0.2000 0.3837 -1.0000 7.0000

11.5345 10.1330 1.0000 0.0000 0.0000 9.9614 6.5316 0.0000

-1.0000 3.5750 143.1770 6.2293 5.2294 0.1542 0.8563 0.0000

-10.2080 2.9867 1.0338 6.2998 2.5791 1.3000 0.2000 13.0000

Si 2.1932 4.0000 28.0600 1.8951 0.1737 0.8112 1.2962 4.0000

11.3429 5.2054 4.0000 21.7115 139.9309 4.0081 5.7104 0.0000

-1.0000 0.0000 128.2031 9.0751 23.8188 0.8381 0.8563 0.0000

-4.1684 2.0754 1.0338 4.0000 2.5791 1.4000 0.2000 13.0000

Al 2.1967 3.0000 26.9820 2.3738 0.2328 0.4558 -1.6836 3.0000

9.4002 3.9009 3.0000 0.0076 16.5151 1.6032 6.7003 0.0000

-1.0000 0.0000 78.4675 20.0000 0.2500 0.0000 0.8563 0.0000

-23.1826 1.5000 1.0338 8.0000 2.5791 1.4000 0.2000 13.0000

Ca 1.9927 2.0000 40.0870 2.7005 0.1848 0.7939 1.0000 2.0000

10.6123 27.5993 3.0000 38.0000 0.0000 -1.9372 6.5275 0.0000

-1.3000 0.0000 220.0000 49.9248 0.3370 0.0000 0.0000 0.0000

-2.0000 4.0000 1.0564 6.2998 2.9663 1.4000 0.0100 13.0000

Na 1.8000 1.0000 22.9898 2.8270 0.1872 0.4000 -1.0000 1.0000

10.0000 2.5000 1.0000 0.0000 0.0000 -1.2155 6.8737 0.0000

-1.0000 0.0000 23.0445 100.0000 1.0000 0.0000 0.8563 0.0000

-2.5000 3.9900 1.0338 8.0000 2.5791 1.4000 0.0100 13.0000

34 ! Nr of bonds; Edis1;LPpen;n.u.;pbe1;pbo5;13corr;pbo6

pbe2;pbo3;pbo4;Etrip;pbo1;pbo2;ovcorr

1 1 158.2004 99.1897 78.0000 -0.7738 -0.4550 1.0000 37.6117 0.4147

0.4590 -0.1000 9.1628 1.0000 -0.0777 6.7268 1.0000 0.0000

1 2 169.4760 0.0000 0.0000 -0.6083 0.0000 1.0000 6.0000 0.7652

5.2290 1.0000 0.0000 1.0000 -0.0500 6.9136 0.0000 0.0000

2 2 153.3934 0.0000 0.0000 -0.4600 0.0000 1.0000 6.0000 0.7300

6.2500 1.0000 0.0000 1.0000 -0.0790 6.0552 0.0000 0.0000

1 3 164.4303 82.6772 60.8077 -0.3739 -0.2351 1.0000 10.5036 1.0000

0.4475 -0.2288 7.0250 1.0000 -0.1363 4.8734 0.0000 0.0000

3 3 142.2858 145.0000 50.8293 0.2506 -0.1000 1.0000 29.7503 0.6051

0.3451 -0.1055 9.0000 1.0000 -0.1225 5.5000 1.0000 0.0000

2 3 160.0000 0.0000 0.0000 -0.5725 0.0000 1.0000 6.0000 0.5626

1.1150 1.0000 0.0000 0.0000 -0.0920 4.2790 0.0000 0.0000

1 4 133.0514 0.0000 0.0000 1.0000 -0.3000 1.0000 36.0000 0.0673

0.2350 -0.3500 15.0000 1.0000 -0.1143 4.5217 1.0000 0.0000

2 4 105.0054 0.0000 0.0000 -0.0717 0.0000 0.0000 6.0000 0.0505

0.1000 1.0000 0.0000 1.0000 -0.1216 4.5062 0.0000 0.0000

3 4 65.7713 0.0000 0.0000 0.1366 -0.3000 1.0000 36.0000 0.0494

0.9495 -0.3500 15.0000 1.0000 -0.0555 7.9897 1.0000 0.0000

4 4 38.7471 0.0000 0.0000 0.3595 -0.2000 0.0000 16.0000 0.2749

1.0000 -0.2000 15.0000 1.0000 -0.0771 6.4477 0.0000 0.0000

2 5 109.1686 0.0000 0.0000 -0.1657 -0.2000 0.0000 16.0000 1.2500

2.8463 -0.2000 15.0000 1.0000 -0.1111 5.2687 0.0000 0.0000

3 5 0.0000 0.0000 0.0000 0.5000 -0.2000 0.0000 16.0000 0.5000

1.0001 -0.2000 15.0000 1.0000 -0.1000 10.0000 0.0000 0.0000

4 5 0.0000 0.0000 0.0000 0.2500 -0.2000 0.0000 16.0000 0.5000

0.5000 -0.2000 15.0000 1.0000 -0.2000 10.0000 0.0000 0.0000

5 5 0.2500 0.0000 0.0000 0.1803 -0.2000 0.0000 16.0000 0.3356

0.9228 -0.2000 15.0000 1.0000 -0.1178 5.6715 0.0000 0.0000

1 6 0.0000 0.0000 0.0000 -0.6528 -0.3000 0.0000 36.0000 0.5000

10.0663 -0.3500 25.0000 1.0000 -0.1000 10.0000 0.0000 0.0000

2 6 250.0000 0.0000 0.0000 -0.7128 0.0000 1.0000 6.0000 0.1186

18.5790 1.0000 0.0000 1.0000 -0.0731 7.4983 0.0000 0.0000

3 6 261.9074 5.9533 0.0000 -0.6223 -0.3000 1.0000 36.0000 0.7275

10.1541 -0.2366 29.7817 1.0000 -0.1083 8.5924 6.0658 0.0000

6 6 70.9120 54.0531 30.0000 0.4931 -0.3000 1.0000 16.0000 0.0392

0.2476 -0.8055 7.1248 1.0000 -0.1009 8.7229 0.0000 0.0000

1 7 0.0000 0.0000 0.0000 -0.6528 -0.3000 0.0000 36.0000 0.5000

10.0663 -0.3500 25.0000 1.0000 -0.1000 10.0000 0.0000 0.0000

2 7 92.8579 0.0000 0.0000 -0.6528 -0.3000 0.0000 36.0000 0.1551

10.0663 -0.3500 25.0000 1.0000 -0.0842 7.1758 0.0000 0.0000

3 7 228.4876 0.0000 0.0000 -0.8524 -0.3000 0.0000 36.0000 0.1252

0.4016 -0.3500 25.0000 1.0000 -0.1750 5.2102 0.0000 0.0000

6 7 0.0000 0.0000 0.0000 1.0000 0.3000 0.0000 26.0000 1.0000

0.5000 0.0000 12.0000 1.0000 -0.2000 10.0000 0.0000 0.0000

7 7 34.0777 0.0000 0.0000 0.4832 -0.3000 0.0000 16.0000 0.5154

6.4631 -0.4197 14.3085 1.0000 -0.1463 6.1608 0.0000 0.0000

2 8 0.0000 0.0000 0.0000 -0.0203 -0.1418 1.0000 13.1260 0.0230

8.2136 -0.1310 0.0000 1.0000 -0.2692 6.4254 0.0000 24.4461

3 8 50.8757 0.0000 43.3991 1.0000 -0.3000 1.0000 36.0000 0.0025

0.7609 -0.2500 12.0000 1.0000 -0.0515 8.9041 1.0000 24.4461

6 8 0.0000 0.0000 0.0000 0.5000 -0.3000 1.0000 16.0000 0.5000

0.5000 -0.2500 15.0000 1.0000 -0.1000 9.0000 0.0000 0.0000

7 8 0.0000 0.0000 0.0000 0.5000 -0.3000 1.0000 16.0000 0.5000

0.5000 -0.2500 15.0000 1.0000 -0.1000 9.0000 0.0000 0.0000

8 8 36.9494 0.0000 0.0000 -0.0412 -0.2000 0.0000 16.0000 0.3233

```
      0.3708  -0.2000  10.0000   1.0000  -0.0822   4.2104   0.0000   0.0000
 2  9   0.0000   0.0000   0.0000  -1.0000  -0.3000   1.0000  36.0000   0.7000
     10.1151  -0.3500  25.0000   1.0000  -0.1053   8.2003   1.0000   0.0000
 3  9  48.5875   0.0000   0.0000  -0.0157  -0.3000   1.0000  36.0000   0.5922
      6.8772  -0.3500  25.0000   1.0000  -0.0630   7.8526   1.0000   0.0000
 6  9   0.1000   0.0000   0.0000   0.2500  -0.5000   1.0000  35.0000   0.6000
      0.5000  -0.5000  20.0000   1.0000  -0.2000  10.0000   1.0000   0.0000
 7  9   0.0000   0.0000   0.0000   0.5000  -0.3000   1.0000  16.0000   0.5000
      0.5000  -0.2500  15.0000   1.0000  -0.1000   9.0000   0.0000   0.0000
 8  9   0.0000   0.0000   0.0000   0.5000  -0.3000   1.0000  16.0000   0.5000
      0.5000  -0.2500  15.0000   1.0000  -0.1000   9.0000   0.0000   0.0000
 9  9  60.0000   0.0000   0.0000  -0.3458   0.3000   0.0000  25.0000   0.2477
      2.4578  -0.4000  12.0000   1.0000  -0.0513   4.5180   0.0000   0.0000
24    ! Nr of off-diagonal terms; Ediss;Ro;gamma;rsigma;rpi;rpi2
 1  2   0.1239   1.4004   9.8467   1.1210  -1.0000  -1.0000
 2  3   0.0283   1.2885  10.9190   0.9215  -1.0000  -1.0000
 1  3   0.1345   1.8422   9.7725   1.2835   1.1576   1.0637
 1  4   0.1358   1.8293  10.0425   1.6096  -1.0000  -1.0000
 2  4   0.0640   1.6974  11.5167   1.3517  -1.0000  -1.0000
 3  4   0.0846   1.4284  10.0808   1.8339  -1.0000  -1.0000
 2  5   0.0568   1.6740   9.6297   1.2200  -1.0000  -1.0000
 3  5   0.1927   2.2551  11.2308  -1.0000  -1.0000  -1.0000
 4  5   0.1500   2.1500  11.0000  -1.0000  -1.0000  -1.0000
 1  6   0.2000   1.9000  12.0000  -1.0000  -1.0000  -1.0000
 2  6   0.2000   1.5207  12.9535   1.2125  -1.0000  -1.0000
 3  6   0.2000   1.9048  10.8374   1.7163   1.2444  -1.0000
 1  7   0.2000   1.9000  12.0000  -1.0000  -1.0000  -1.0000
 2  7   0.0564   1.4937  12.0744   1.7276  -1.0000  -1.0000
 3  7   0.1651   1.8998  11.2212   1.5416  -1.0000  -1.0000
```

6 7 0.0216 1.5025 11.8792 -1.0000 -1.0000 -1.0000

1 8 0.1000 1.9000 11.5000 -1.0000 -1.0000 -1.0000

2 8 0.0100 1.6000 13.2979 -1.0000 -1.0000 -1.0000

3 8 0.0955 1.7587 11.9417 1.9052 -1.0000 -1.0000

6 8 0.1000 1.9000 11.0000 -1.0000 -1.0000 -1.0000

7 8 0.1000 1.9000 11.0000 -1.0000 -1.0000 -1.0000

3 9 0.1574 1.5000 11.8005 1.5685 -1.0000 -1.0000

6 9 0.1315 2.0482 17.5616 -1.0000 -1.0000 -1.0000

7 9 0.1315 2.0482 17.5616 -1.0000 -1.0000 -1.0000

69 ! Nr of angles;at1;at2;at3;Thetao,o;ka;kb;pv1;pv2

1 1 1 59.0573 30.7029 0.7606 0.0000 0.7180 6.2933 1.1244

1 1 2 65.7758 14.5234 6.2481 0.0000 0.5665 0.0000 1.6255

2 1 2 70.2607 25.2202 3.7312 0.0000 0.0050 0.0000 2.7500

1 2 2 0.0000 0.0000 6.0000 0.0000 0.0000 0.0000 1.0400

1 2 1 0.0000 3.4110 7.7350 0.0000 0.0000 0.0000 1.0400

2 2 2 0.0000 27.9213 5.8635 0.0000 0.0000 0.0000 1.0400

1 1 3 53.9517 7.8968 2.6122 0.0000 3.0000 58.6562 1.0338

3 1 3 76.9627 44.2852 2.4177 -25.3063 1.6334 -50.0000 2.7392

2 1 3 65.0000 16.3141 5.2730 0.0000 0.4448 0.0000 1.4077

1 3 1 72.6199 42.5510 0.7205 0.0000 2.9294 0.0000 1.3096

1 3 3 81.9029 32.2258 1.7397 0.0000 0.9888 68.1072 1.7777

3 3 3 80.7324 30.4554 0.9953 0.0000 3.0000 50.0000 1.0783

1 3 2 70.1101 13.1217 4.4734 0.0000 0.8433 0.0000 3.0000

2 3 3 75.6935 50.0000 2.0000 0.0000 1.0000 0.0000 1.1680

2 3 2 85.8000 9.8453 2.2720 0.0000 2.8635 0.0000 1.5800

1 2 3 0.0000 25.0000 3.0000 0.0000 1.0000 0.0000 1.0400

3 2 3 0.0000 15.0000 2.8900 0.0000 0.0000 0.0000 2.8774

2 2 3 0.0000 8.5744 3.0000 0.0000 0.0000 0.0000 1.0421

1 4 1 29.1655 3.3035 0.2000 0.0000 1.1221 0.0000 1.0562

1 1 4 59.8697 2.8115 1.9262 0.0000 0.7602 0.0000 1.4056

1 4 4 25.4591 15.9430 0.9664 0.0000 2.2242 0.0000 1.1088

4 1 4 88.6279 26.0015 1.0328 0.0000 0.2361 0.0000 2.0576

2 1 4 47.3695 16.9204 4.1052 0.0000 0.1000 0.0000 1.0050

2 4 2 34.1965 6.6782 6.5943 0.0000 1.3895 0.0000 1.5365

2 2 4 0.1000 30.0000 3.4094 0.0000 2.4379 0.0000 1.5166

4 2 4 0.0000 8.2994 5.7832 0.0000 2.9873 0.0000 1.7716

2 4 4 21.2590 6.5954 0.9951 0.0000 2.8006 0.0000 1.0000

2 4 4 180.0000 -6.9970 24.3956 0.0000 0.7878 0.0000 1.3672

1 3 4 90.0000 12.8684 1.4601 0.0000 0.8757 0.0000 1.0000

3 1 4 18.8567 24.3753 3.9647 0.0000 0.1000 0.0000 1.5314

3 4 3 79.7335 0.0100 0.1392 0.0000 0.4968 0.0000 2.1948

4 3 4 57.6787 4.8566 2.5768 0.0000 0.7552 0.0000 1.0000

2 3 4 59.4556 10.2025 0.7481 0.0000 1.4521 0.0000 1.0000

3 3 4 73.6721 32.6330 1.7223 0.0000 1.0221 0.0000 1.4351

3 4 4 65.7545 5.6268 4.0645 0.0000 1.7794 0.0000 2.6730

3 2 4 0.0000 4.6026 2.5343 0.0000 0.7284 0.0000 1.1051

2 4 3 34.0653 20.1868 4.7461 0.0000 0.1000 0.0000 1.6752

3 2 5 0.0000 0.0100 0.5211 0.0000 0.0000 0.0000 1.3859

6 6 6 78.5339 36.4328 1.0067 0.0000 0.1694 0.0000 1.6608

2 6 6 77.2616 5.0190 7.8944 0.0000 4.0000 0.0000 1.0400

2 6 2 75.7983 14.4132 2.8640 0.0000 4.0000 0.0000 1.0400

3 6 6 90.6812 31.1846 4.4543 0.0000 0.5073 0.0000 2.1809

2 6 3 73.6998 40.0000 1.8782 0.0000 4.0000 0.0000 1.1290

3 6 3 80.1361 36.2368 0.9504 0.0000 0.2624 0.0000 2.0787

6 3 6 80.4450 6.0739 1.7731 0.0000 3.2548 0.0000 1.0422

2 3 6 86.7611 7.1742 1.4013 0.0000 1.4999 0.0000 1.0400

3 3 6 103.4529 26.9589 1.3470 0.0000 1.7728 0.0000 1.3091

2 2 6 0.0000 47.1300 6.0000 0.0000 1.6371 0.0000 1.0400

```
 6  2  6   0.0000  27.4206   6.0000   0.0000   1.6371   0.0000   1.0400
 3  2  6   0.0000   5.0000   1.0000   0.0000   1.0000   0.0000   1.2500
 3  2  7   0.0000   4.2750   1.0250   0.0000   1.3750   0.0000   1.4750
 2  2  7   0.0000   3.0000   1.0000   0.0000   1.0000   0.0000   1.2500
 7  2  7   0.0000  20.2391   0.1328   0.0000   2.9860   0.0000   1.0870
 2  3  7  88.1144  13.2143   1.5068   0.0000   3.0000   0.0000   1.0100
 3  3  7  34.4326  25.9544   5.1239   0.0000   2.7500   0.0000   1.7141
 7  3  7  21.6945  20.0000   4.0000   0.0000   0.6619   0.0000   1.9714
 2  7  2  67.4229   4.5148   5.9702   0.0000   3.0000   0.0000   2.6879
 2  7  3  41.8108  17.3800   2.6618   0.0000   0.7372   0.0000   1.0100
 3  7  3  49.1145  11.8902   2.1383   0.0000   3.0000   0.0000   1.4790
 2  7  7 180.0000 -26.7860   7.3549   0.0000   1.0000   0.0000   1.0252
 2  7  7  78.2279  37.6504   0.4809   0.0000   1.0000   0.0000   2.9475
 6  3  7  16.5023   0.0100   2.7027   0.0000   1.0000   0.0000   1.0000
 3  6  7  88.2703   0.3954   0.2500   0.0000   0.5000   0.0000   2.1060
 3  7  6  83.8306   0.3712   0.2500   0.0000   0.5000   0.0000   2.1153
 3  8  3   1.0000   4.9611   2.4541   0.0000   0.5754   0.0000   1.0000
 8  3  8   9.5066   4.2640   3.1438   0.0000   1.9819   0.0000   1.6463
 2  3  8  51.3829   2.5000   0.2500   0.0000   0.0500   0.0000   1.0000
 3  3  8  70.0000  25.0000   1.0000   0.0000   1.0000   0.0000   1.2500
 2  3  9  72.0932   5.0000   1.0000   0.0000   1.0009   0.0000   1.2500
32    ! Nr of torsions;at1;at2;at3;at4;;V1;V2;V3;V2(BO);vconj;n.u;n
 1  1  1  1  -0.2500  34.7453   0.0288  -6.3507  -1.6000   0.0000   0.0000
 1  1  1  2  -0.2500  29.2131   0.2945  -4.9581  -2.1802   0.0000   0.0000
 2  1  1  2  -0.2500  31.2081   0.4539  -4.8923  -2.2677   0.0000   0.0000
 1  1  1  3   1.2799  20.7787  -0.5249  -2.5000  -1.0000   0.0000   0.0000
 2  1  1  3   1.9159  19.8113   0.7914  -4.6995  -1.0000   0.0000   0.0000
 3  1  1  3  -1.4477  16.6853   0.6461  -4.9622  -1.0000   0.0000   0.0000
 1  1  3  1   0.4816  19.6316  -0.0057  -2.5000  -1.0000   0.0000   0.0000
```

1 1 3 2 1.2044 80.0000 -0.3139 -6.1481 -1.0000 0.0000 0.0000

2 1 3 1 -2.5000 31.0191 0.6165 -2.7733 -2.9807 0.0000 0.0000

2 1 3 2 -2.4875 70.8145 0.7582 -4.2274 -3.0000 0.0000 0.0000

1 1 3 3 -0.3566 10.0000 0.0816 -2.6110 -1.9631 0.0000 0.0000

2 1 3 3 -1.4383 80.0000 1.0000 -3.6877 -2.8000 0.0000 0.0000

3 1 3 1 -1.1390 78.0747 -0.0964 -4.5172 -3.0000 0.0000 0.0000

3 1 3 2 -2.5000 70.3345 -1.0000 -5.5315 -3.0000 0.0000 0.0000

3 1 3 3 -2.0234 80.0000 0.1684 -3.1568 -2.6174 0.0000 0.0000

1 3 3 1 1.1637 -17.3637 0.5459 -3.6005 -2.6938 0.0000 0.0000

1 3 3 2 -2.1289 12.8382 1.0000 -5.6657 -2.9759 0.0000 0.0000

2 3 3 2 2.5000 -22.9397 0.6991 -3.3961 -1.0000 0.0000 0.0000

1 3 3 3 2.5000 -25.0000 1.0000 -2.5000 -1.0000 0.0000 0.0000

2 3 3 3 -2.5000 -2.5103 -1.0000 -2.5000 -1.0000 0.0000 0.0000

3 3 3 3 -2.5000 -25.0000 1.0000 -2.5000 -1.0000 0.0000 0.0000

0 1 2 0 0.0000 0.0000 0.0000 0.0000 0.0000 0.0000 0.0000

0 2 2 0 0.0000 0.0000 0.0000 0.0000 0.0000 0.0000 0.0000

0 2 3 0 0.0000 0.1000 0.0200 -2.5415 0.0000 0.0000 0.0000

0 1 1 0 0.0000 50.0000 0.3000 -4.0000 -2.0000 0.0000 0.0000

0 3 3 0 0.5511 25.4150 1.1330 -5.1903 -1.0000 0.0000 0.0000

1 1 3 3 -0.0002 20.1851 0.1601 -9.0000 -2.0000 0.0000 0.0000

1 3 3 1 0.0002 80.0000 -1.5000 -4.4848 -2.0000 0.0000 0.0000

3 1 3 3 -0.1583 20.0000 1.5000 -9.0000 -2.0000 0.0000 0.0000

2 6 6 2 0.0000 0.0000 0.0640 -2.4426 0.0000 0.0000 0.0000

2 6 6 6 0.0000 0.0000 0.1587 -2.4426 0.0000 0.0000 0.0000

0 2 6 0 0.0000 0.0000 0.1200 -2.4847 0.0000 0.0000 0.0000

1 ! Nr of hydrogen bonds;at1;at2;at3;Rhb;Dehb;vhb1

3 2 3 2.1200 -3.5800 1.4500 19.5000

REFERENCES

[1] J.H. Lee, Y.F. Gao, K.E. Johanns, G.M. Pharr, Cohesive interface simulations of indentation cracking as a fracture toughness measurement method for brittle materials, Acta Materialia. 60 (2012) 5448–5467. https://doi.org/10.1016/j.actamat.2012.07.011.

[2] K.E. Johanns, J.H. Lee, Y.F. Gao, G.M. Pharr, An evaluation of the advantages and limitations in simulating indentation cracking with cohesive zone finite elements, Modelling Simul. Mater. Sci. Eng. 22 (2013) 015011. https://doi.org/10.1088/0965-0393/22/1/015011.

[3] M.L. Oyen, R.F. Cook, A practical guide for analysis of nanoindentation data, Journal of the Mechanical Behavior of Biomedical Materials. 2 (2009) 396–407. https://doi.org/10.1016/j.jmbbm.2008.10.002.

[4] R. Huang, N. Sukumar, J.-H. Prévost, Modeling quasi-static crack growth with the extended finite element method Part II: Numerical applications, International Journal of Solids and Structures. 40 (2003) 7539–7552. https://doi.org/10.1016/j.ijsolstr.2003.08.001.

[5] N. Sukumar, J.-H. Prévost, Modeling quasi-static crack growth with the extended finite element method Part I: Computer implementation, International Journal of Solids and Structures. 40 (2003) 7513–7537. https://doi.org/10.1016/j.ijsolstr.2003.08.002.

[6] M. Stolarska, D.L. Chopp, N. Moës, T. Belytschko, Modelling crack growth by level sets in the extended finite element method, International Journal for Numerical Methods in Engineering. 51 (2001) 943–960. https://doi.org/10.1002/nme.201.

[7] M. Smith, ABAQUS/Standard User's Manual, Version 6.9, Dassault Systèmes Simulia Corp, United States, 2009.

[8] G. Papazafeiropoulos, M. Muñiz-Calvente, E. Martínez-Pañeda, Abaqus2Matlab: A suitable tool for finite element post-processing, Advances in Engineering Software. 105 (2017) 9–16. https://doi.org/10.1016/j.advengsoft.2017.01.006.

[9] S. Das, A. Maroli, S.S. Singh, T. Stannard, X. Xiao, N. Chawla, N. Neithalath, A microstructure-guided constitutive modeling approach for random heterogeneous materials: Application to structural binders, Computational Materials Science. 119 (2016) 52–64. https://doi.org/10.1016/j.commatsci.2016.03.040.

[10] S. Das, P. Yang, S.S. Singh, J.C.E. Mertens, X. Xiao, N. Chawla, N. Neithalath, Effective properties of a fly ash geopolymer: Synergistic application of X-ray synchrotron tomography, nanoindentation, and homogenization models, Cement and Concrete Research. 78 (2015) 252–262. https://doi.org/10.1016/j.cemconres.2015.08.004.

[11] T. Mori, K. Tanaka, Average stress in matrix and average elastic energy of materials with misfitting inclusions, Acta Metallurgica. 21 (1973) 571–574. https://doi.org/10.1016/0001-6160(73)90064-3.